Scott M. Chadderdon,[1] J. Todd Belcik,[1] Lindsay Bader,[2] Dawn M. Peters,[1] Paul Kievit,[2] Nabil J. Alkayed,[1] Sanjiv Kaul,[1] Kevin L. Grove,[2] and Jonathan R. Lindner[1]

Temporal Changes in Skeletal Muscle Capillary Responses and Endothelial-Derived Vasodilators in Obesity-Related Insulin Resistance

Diabetes 2016;65:2249–2257 | DOI: 10.2337/db15-1574

The inability of insulin to increase skeletal muscle capillary blood volume (CBV) reduces glucose uptake in insulin resistance (IR). We hypothesized that abnormalities in endothelial-derived vasodilator pathways are temporally associated with the development of IR and an impaired ability to increase skeletal muscle CBV. A comprehensive metabolic and vascular screening assessment was performed on 10 adult rhesus macaques at baseline and every 4–6 months for 2 years after starting a high-fat diet supplemented with fructose. Diet changes resulted in an 80% increase in truncal fat by 4 months. Hyperinsulinemia and decreased glucose utilization were observed from 4 to 18 months. At 24 months, pancreatic secretory function and the glucose utilization rate declined. CBV at rest and during an intravenous glucose tolerance test demonstrated a sustained increase from 4 to 18 months and then abruptly fell at 24 months. Nitric oxide bioavailability progressively decreased over 2 years. Conversely, endothelial-derived vasodilators progressively increased over 18 months and then abruptly decreased at 24 months in concert with the CBV. The increase in basal and glucose-mediated CBV early in IR may represent a compensatory response through endothelial-derived vasodilator pathways. The inability to sustain a vascular compensatory response limits glucose-mediated increases in CBV, which correlates with the severity of IR.

In healthy subjects, increases in serum insulin within and above the physiologic range increase skeletal muscle blood flow (1). This response is mediated primarily through insulin receptor signaling and Akt-mediated activation of endothelial nitric oxide (NO) synthase (eNOS) (2–4). The resulting increase in NO production leads to changes in precapillary arteriolar tone and a rapid expansion in the number of capillaries perfused.

Insulin-mediated capillary recruitment is important for increasing the vascular surface area for insulin and glucose delivery and subsequent muscle glucose uptake (5–7). Techniques capable of quantifying skeletal muscle blood flow and capillary blood volume (CBV) have indicated that insulin-mediated capillary recruitment is impaired in obesity and insulin resistance (IR) (8–10). Vascular IR, defined as impaired insulin-induced phosphorylation of Akt and eNOS, has been shown to precede the onset of skeletal muscle and hepatocellular IR in models of diet-induced obesity (11). Together, these findings suggest that abnormalities in vascular function could represent an early link between obesity and IR.

There remain unanswered questions regarding the causative link between obesity, microvascular dysfunction, and IR. Importantly, the temporal course of abnormal skeletal muscle capillary function has not been defined in clinically relevant models of obesity. Furthermore, the effect of a high-fat diet (HFD) on NO bioavailability and the endothelial-derived hyperpolarizing factors (EDHF) in the epoxyeicosatrienoic acid (EET) family of metabolites may have significant physiologic contributions because they have been implicated in regulating skeletal muscle CBV (8,12). In this study, we hypothesized that impairments in skeletal muscle microvascular blood flow and CBV associated with diet-induced IR in nonhuman primates would coincide with alterations in NO-mediated vasodilation and EDHFs, including cytochrome P450–derived EETs, soluble epoxide-hydrolase–derived dihydroxyeicosatrienoic acids (DHETs),

[1]Knight Cardiovascular Institute, Oregon Health & Science University, Portland, OR
[2]Oregon National Primate Research Center, Oregon Health & Science University, Portland, OR

Corresponding author: Scott M. Chadderdon, chadderd@ohsu.edu.

Received 13 November 2015 and accepted 5 April 2016.

See accompanying article, p. 2118.

and lipoxygenase-derived 12- and 15-hydroxyeicosatetraenoic acids (HETEs) (13–15).

RESEARCH DESIGN AND METHODS

Primate Study Design

The study was approved by the Oregon National Primate Research Center Animal Care and Use Committee at Oregon Health & Science University and conformed to the U.S. Department of Agriculture and the Association for Assessment and Accreditation of Laboratory Animal Care guidelines for nonhuman primate care. Ten adult male rhesus macaques (*Macaca mulatta*), 9–11 years of age, were studied while on a standard diet composed of 58% carbohydrates, 27% protein, and 15% fat by caloric content. Animals were restudied at 4, 8, 12, 18, and 24 months after starting an HFD consisting of 46% carbohydrates, 18% protein, and 36% fat by caloric content and supplemented with a 100-g fructose drink four times weekly. During follow-up, two animals were removed from the protocol after 18 months to fulfill alternative studies.

The following tests were performed at each interval: intravenous glucose tolerance test (IVGTT), DEXA, venous blood samples for plasma EETs, DHETs, and HETEs, brachial artery flow-mediated vasodilation (FMD), and contrast-enhanced ultrasound (CEU) skeletal muscle perfusion imaging at rest and during a glucose challenge to assess functional capillary recruitment.

A separate cohort of five obese primates (12 ± 1.5 years) underwent an additional 2-day study protocol after 33 ± 8 months on the HFD. On day 1, CEU skeletal muscle perfusion was performed at rest and during a glucose challenge. On day 2, CEU skeletal muscle perfusion studies were repeated during a fluconazole infusion to inhibit endothelial production of EETs and HETEs (16–18).

For all protocols, primates were studied after an overnight fast. Telazol (5 mg/kg i.m.) was used for sedation during IVGTTs and DEXA scans. Ketamine (10 mg/kg i.m.) and isoflurane (1.0–1.5%) were used for sedation and anesthesia during ultrasound studies.

IVGTT

After an overnight fast, animals received dextrose (600 mg/kg i.v.) over 1 min. Venous blood samples were obtained at 0, 1, 3, 5, 10, 20, 40, and 60 min after dextrose injection for measurement of blood glucose (FreeStyle; Abbott Laboratories) and plasma insulin concentration (Immulite 2000; Siemens Medical Systems). The 1-hour IVGTT and glucose dose was based on extensive experience with this algorithm in rhesus macaques (19–21). The following parameters were obtained from the IVGTT: *1*) HOMA-IR = (basal glucose mg/dL × basal insulin μIU/mL)/405; *2*) 0–60 min insulin area under the curve (AUC) concentration; *3*) acute insulin response (AIR) = 1–10 min average insulin concentration; and *4*) glucose disappearance rate (K_G) = (Ln [20 min glucose] – Ln [5 min glucose]/15 min × 100%) as a parameter for insulin sensitivity (21,22). Insulin AUC and K_G data have been previously reported (20). From the IVGTT, a disposition index (DI) was calculated as AIR × K_G. Previous studies using the AIR and various measures of insulin sensitivity to calculate the DI have been shown to predict the development of type 2 diabetes in high-risk groups (23).

DEXA

Body composition was assessed by DEXA (Discovery A; Hologic, Inc.) to obtain lean mass and fat mass. Percentage of truncal fat was calculated as (truncal fat mass/total truncal mass). Body weight and percentage of truncal fat data have been previously reported (20).

Plasma Lipids, HbA_{1c}, and Eicosanoid Metabolites

Venous blood samples were collected under anesthesia for fasting plasma lipids and HbA_{1c}, as previously reported (20). Separate plasma samples were obtained, and liquid-chromatography/mass spectrometry was performed for EETs *cis*-regioisomers (14,15-, 11,12-, and 8,9-EET), their corresponding hydrolyzed DHETs (14,15-, 11,12-, and 8,9-DHET), and HETEs (12-, 15-, 18-, 19-, and 20-HETE).

FMD

FMD of the brachial artery was performed to assess NO bioavailability and has been previously reported (20).

Skeletal Muscle Perfusion and Functional CBV

CEU skeletal muscle imaging of the proximal calf muscles was performed at rest and after the administration of a dextrose bolus (600 mg/kg over 1 min) to assess changes in microvascular blood flow and functional capillary recruitment, as previously reported (8).

Inhibition of Eicosanoid Synthesis

Eicosanoid synthesis was inhibited by an intravenous infusion of fluconazole (2 mg/mL) at 0.05 mL/kg/min starting 45 min before the CEU studies in the second group of primates. The dose of fluconazole used was four times higher than that reported in human studies that suppressed eicosanoids by 5–16% (24). Venous blood samples were collected immediately before baseline CEU to assess plasma fluconazole levels by ultra-performance liquid chromatography/mass spectrometry (University of Texas Health Science Center Fungus Testing Laboratory). Plasma samples for EETs, DHETs, and HETEs were collected before and at the completion of the fluconazole infusion.

Statistical Methods

Data were analyzed by Prism 5.0 software (GraphPad Software, Inc.) and Stata 11.2 software (StataCorp LP). Summary information is expressed as mean ± SEM. Owing to the longitudinal study nature and the withdrawal of two primates from the study protocol after 18 months, data were analyzed across the 24-month period with longitudinal mixed models. For standardization of data analysis, we assessed whether the observed changes over time were linear or had curvature and fit a quadratic function. If the data fit a quadratic function, then stepwise tests were performed to assess the significance of changes between 0 and 4 months, 4 and 18 months, and then 18 and 24 months.

After this stepwise testing, Holm correction was applied for multiple testing. In the absence of a significant quadratic effect at level 0.05, linear terms were tested, and multiple comparisons were not performed because the linear fit implies that each time point is significantly different from each other. When neither the quadratic nor linear models were significant at $P < 0.05$, unstructured models were fit and compared in the same stepwise fashion as above. Unstructured models were used only for the DI data. The analysis of capillary blood flow and CBV with fluconazole testing was analyzed with mixed models with a heterogeneous compound symmetric covariance matrix. The average 12- and 15-HETE and the average 18-, 19-, and 20-HETE data in primates exposed to fluconazole were analyzed with a Wilcoxon matched-pairs signed rank test, and the average EETs and DHETs were analyzed with a paired, Student *t* test.

RESULTS

Early Response to the HFD (4 Months)

At 4 months, the daily caloric intake increased by 68% when converting to the HFD (711 ± 167 kcal/day vs. 1,195 ± 67 kcal/day, $P < 0.01$). The diet change did not alter the primates' average daily activity levels across the study time points. Systolic and diastolic blood pressure and lipids were increased after 4 months and have been previously reported (20). Body weight, glucose and insulin homeostasis, and DI in response to the HFD are provided in Table 1. By 4 months, body mass increased by 20%, whereas truncal fat increased by nearly 80%. These changes were associated with nearly doubling of the basal insulin levels and basal IR as measured by HOMA-IR. Small but significant changes were noted in basal glucose and HbA_{1c} values. Figure 1 illustrates the temporal changes in the insulin responsiveness and the K_G data as a measure of insulin sensitivity. At 4 months, there was a marked increase in the insulin AUC concentration and in the AIR and a simultaneous decline in the K_G. Together, these features of a hyperinsulinemic response with impaired glucose clearance indicate the development of obesity-related IR.

Despite the rise in blood pressure, plasma lipids, abdominal obesity, and IR, resting and glucose-stimulated skeletal muscle microvascular blood flow increased in the first 4 months of the HFD (Fig. 2*A*). This change was attributable to a rise in the basal and in the glucose-stimulated CBV (Fig. 2*B*), whereas the respective microvascular blood flux rates, β values, were unchanged (data not shown).

After 4 months of the HFD, there were no significant changes in eicosanoid-derived vasoconstrictors (18-, 19-, and 20-HETE) or in the cytochrome P450–derived vasodilator EETs (8,9-, 11,12-, and 14,15-EET) and corresponding DHETs (Fig. 2*C* and Table 2 for individual eicosanoid concentrations). NO bioavailability was unchanged, whereas a small but significant increase was noted in lipoxygenase-derived 12- and 15-HETE vasodilators ($P = 0.04$, Holm corrected $P = 0.13$) (Fig. 2*D*).

Intermediate Response to the HFD (4 to 18 Months)

Caloric intake was unchanged from 4 to 12 months and not recorded thereafter. From 4 to 18 months, there were slight but significant increases in total body weight and percentage of truncal fat. Mild increases were also noted in basal glucose and HbA_{1c}, with more substantial increases in basal insulin and HOMA-IR (Table 1). Despite the increase in body mass, abdominal obesity, and basal insulin during this period, no further significant changes were noted in the overall insulin AUC response, the AIR, or the K_G (Fig. 1).

This stable phase of IR from 4 to 18 months was mirrored by a stable phase of skeletal muscle microvascular blood flow and CBV at rest and after a glucose bolus (Fig. 2*A* and *B*), with no changes in eicosanoid-derived vasoconstrictors (Fig. 2*C*). There were significant increases in the cytochrome P450–derived vasodilator EETs and DHETs (8,9-, 11,12-, and 14,15-DHET) and a nonsignificant trend for an increase in the lipoxygenase-derived 12- and 15-HETE vasodilators (Fig. 2*C* and *D*). Conversely, there was a significant progressive decline in FMD from 4 to 18 months (Fig. 2*D*). These data suggest that an increase in the endothelial-derived eicosanoid vasodilators (cytochrome P450– and lipoxygenase-derived pathways) may compensate

Table 1—Weight, glucose, HOMA-IR, and DI in response to the HFD

	Baseline *n* = 10	4 months *n* = 10	8 months *n* = 10	12 months *n* = 10	18 months *n* = 10	24 months *n* = 8	Quadratic term or linear* *P* value
Weight, kg	11.0 ± 0.6	13.2 ± 0.8‡	13.5 ± 0.9	13.7 ± 0.9	14.5 ± 0.8‡	14.1 ± 0.8	<0.05
Truncal fat, %	19.1 ± 3.0	34.0 ± 3.4‡	34.4 ± 3.4	36.6 ± 3.5	40.4 ± 3.1‡	38.3 ± 2.9‡	<0.01
Basal insulin, μIU/mL	17 ± 3	32 ± 12	33 ± 11	32 ± 7	48 ± 13	33 ± 11	<0.01*
HOMA-IR	2.4 ± 0.5	5.3 ± 1.9	5.9 ± 1.9	5.3 ± 3.8	8.3 ± 2.7	5.6 ± 1.7	<0.01*
Basal glucose, mg/dL	58 ± 2	68 ± 2	74 ± 3	64 ± 2	67 ± 3	73 ± 3	<0.01*
HbA_{1c}, %	6.2 ± 0.3	6.3 ± 0.1	6.5 ± 0.1	6.6 ± 0.3	6.7 ± 0.1	6.6 ± 0.1	<0.01*
HbA_{1c}, mmol/mol	44 ± 4	45 ± 1	47 ± 1	49 ± 3	50 ± 1	49 ± 1	<0.01*
DI, μIU/mL × %/min	313 ± 64	499 ± 172	548 ± 165	523 ± 130	499 ± 83	349 ± 127	0.10†

Data are mean ± SEM. ‡Quadratic fit $P < 0.05$ with Holm correction $P < 0.05$. *Fits linear model, each point significantly different. †Does not fit either quadratic or linear term.

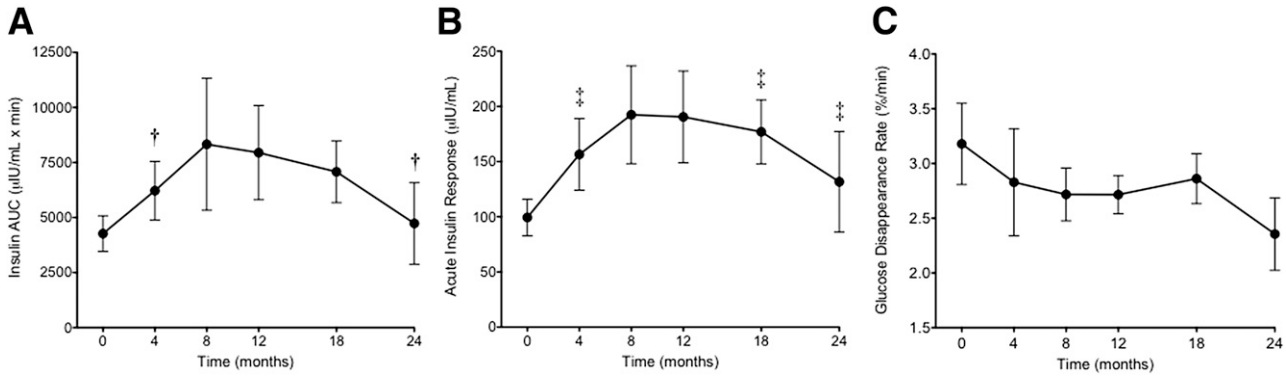

Figure 1—Measures of IR and insulin sensitivity in rhesus macaques at baseline and during follow-up after initiating the HFD. Insulin concentration AUC (*A*), AIR (*B*), and K_G (*C*). †Quadratic fit $P < 0.05$ with Holm correction $P > 0.05$. ‡Quadratic fit $P < 0.05$ with Holm correction $P < 0.05$.

for the loss of NO bioavailability and may contribute to stabilizing the vascular response to insulin.

Late Response to the HFD (18 to 24 Months)

After 24 months, weight and abdominal fat content both remained elevated above baseline values but fell in comparison with 18 months in the eight remaining primates. There was also a decline in basal insulin and HOMA-IR and an increase in the basal blood glucose concentration (Table 1). During IVGTT, there was a decrease in total insulin AUC and AIR (Fig. 1*A* and *B*) and a nonsignificant trend for a decrease in K_G (Fig. 1*C*). A nonsignificant reduction was also noted in the DI (Table 1).

Skeletal muscle microvascular blood flow at rest and in response to a glucose bolus were both significantly decreased at 24 months compared with 18 months (Fig. 2*A* and *B*).

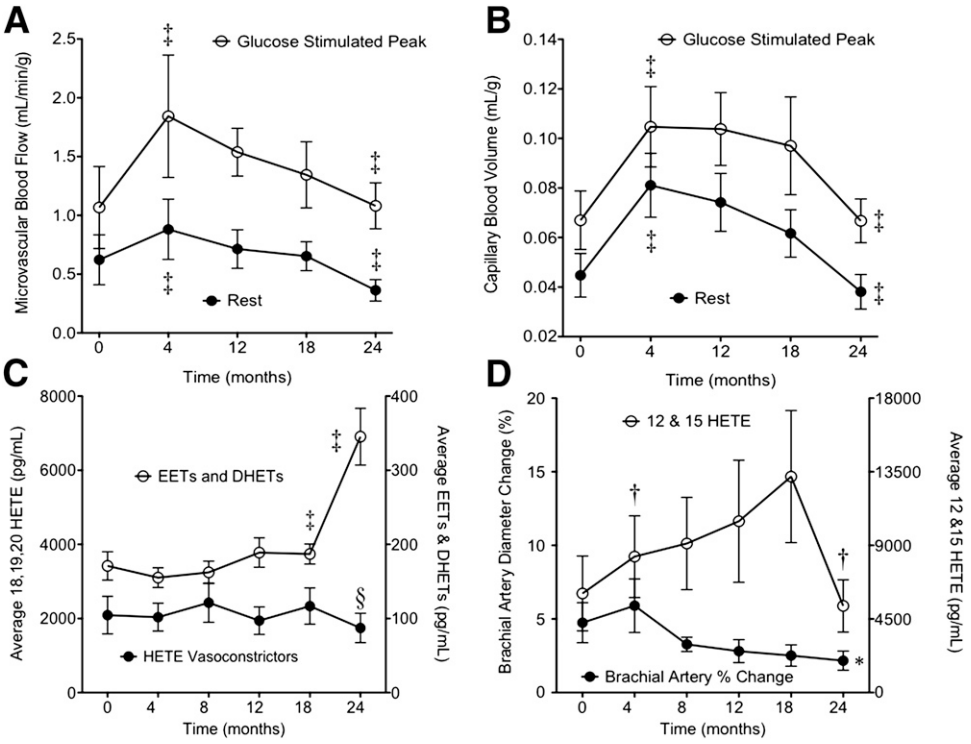

Figure 2—Skeletal muscle microvascular perfusion and mediators of vasomotor tone measured in rhesus macaques at baseline and during follow-up after initiating the HFD. Microvascular blood flow (*A*) and CBV (*B*). *C*: Average plasma concentration of eicosanoid vasoconstrictors (18-, 19-, and 20-HETE) (left *y*-axis) and average plasma concentration of eicosanoid vasodilators (8,9-,11,12-, and 14,15-EETs and corresponding DHETs) (right *y*-axis). *D*: Percentage of brachial artery dilation during FMD (left *y*-axis) and plasma concentration of eicosanoid vasodilators 12- and 15-HETE (right *y*-axis). ‡Quadratic fit $P < 0.05$ with Holm correction $P < 0.05$. §Unstructured model $P < 0.05$. †Quadratic fit $P < 0.05$ with Holm correction $P > 0.05$. *Fits linear model, each point significantly different.

Table 2—Temporal change in eicosanoid vasodilators in response to HFD

Metabolite	Baseline	4 months	8 months	12 months	18 months	24 months	Quadratic term or linear* *P* value
Avg HETE, ng/mL	6.06 ± 2.29	8.31 ± 2.50†	9.12 ± 2.82	10.5 ± 3.73	13.2 ± 4.04	5.30 ± 1.60†	0.04
12-HETE, ng/mL	11.5 ± 3.93	15.8 ± 3.7†	17.4 ± 4.29	19.8 ± 6.27	25.0 ± 6.14	10.1 ± 2.08†	0.04
15-HETE, ng/mL	0.61 ± 0.19	0.81 ± 0.21†	0.84 ± 0.24	1.18 ± 0.43	1.38 ± 0.31	0.48 ± 0.12†	0.02
Avg EET and DHET, pg/mL	171 ± 19	155 ± 13	162 ± 15	189 ± 20	187 ± 14‡	345 ± 38‡	<0.01
8,9-EET, pg/mL	66 ± 8	59 ± 9‡	59 ± 7	69 ± 7	141 ± 21‡	387 ± 61‡	<0.01
8,9-DHET, pg/mL	119 ± 31	96 ± 6	88 ± 6	106 ± 9	81 ± 9	75 ± 4	<0.01*
11,12-EET, pg/mL	79 ± 9	78 ± 12	73 ± 8	89 ± 9	153 ± 26‡	462 ± 78‡	<0.01
11,12-DHET, pg/mL	285 ± 63	240 ± 16	227 ± 17	242 ± 21	204 ± 24	180 ± 10	<0.01*
14,15-EET, pg/mL	141 ± 10	145 ± 21	232 ± 50	307 ± 84	242 ± 36	698 ± 119	<0.01*
14,15-DHET, pg/mL	336 ± 47	314 ± 14	294 ± 20	323 ± 18	301 ± 26	270 ± 13	<0.01*

Data are mean ± SEM. Avg, average. ‡Quadratic fit $P < 0.05$ with Holm correction $P < 0.05$. †Quadratic fit $P < 0.05$ with Holm correction $P > 0.05$. *Fits linear model, each point significantly different.

This change in microvascular blood flow was attributable to significant reductions in the rest and glucose-stimulated CBV. Between 18 and 24 months there was an increase in the cytochrome P450–derived eicosanoid vasodilators but an abrupt decline in the lipoxygenase-derived 12- and 15-HETE vasodilators ($P = 0.04$, Holm corrected $P = 0.13$), leading to an overall decrease in eicosanoid vasodilator concentrations (Fig. 2*C* and *D* and Table 2 for individual eicosanoid concentrations).

The overall 24-month pattern of metabolic data, skeletal muscle CBV, and vasodilator and vasoconstrictor profiles suggests that eicosanoid-derived vasodilator concentrations may serve as a compensatory response to obesity to increase the skeletal muscle CBV and participate in stabilizing the degree of IR. The simultaneous fall in the eicosanoid-derived vasodilator concentrations and the skeletal muscle CBV at 24 months suggests that the loss of this vascular compensatory response, along with the first signs of pancreatic insufficiency, contributes to the severity of IR.

Skeletal Muscle Microvascular Response to Glucose During Eicosanoid Inhibition

A separate cohort of five obese primates on the HFD (age-matched to the prior cohort) was studied to assess the effect of eicosanoid inhibition on basal and glucose-stimulated skeletal muscle blood flow and CBV. The metabolic profile of these primates is noted in Table 3. The fluconazole plasma concentration before starting the IVGTT was 11.4 ± 1.8 μg/mL and above the expected human peak plasma range of 4–8 μg/mL after a 400-mg oral dose (25). Treatment with fluconazole resulted in attenuation of the microvascular blood flow and CBV responses to a glucose bolus compared with studies performed in the absence of fluconazole a day prior (Fig. 3*A* and *B*). Fluconazole produced an acute reduction in lipoxygenase-derived 12- and 15-HETE vasodilators and in 18-, 19-, and 20-HETE vasoconstrictor concentrations, whereas cytochrome P450–derived vasodilator EETs (8,9-, 11,12-, and 14,15-EET) and their corresponding DHETs were unchanged (Fig. 3*C–E*). Individual responses are provided in Fig. 4 to appreciate the effect of fluconazole on 12- and 15-HETE and the relationship to glucose-stimulated CBV. A paradoxical rise in 12- and 15-HETE associated with the highest glucose-stimulated muscle CBV was noted in one animal. In all other animals, fluconazole reduced 12- and 15-HETE concentrations with an associated low glucose-stimulated CBV.

Temporal associations were noted in the rise and fall of 12- and 15-HETE and the glucose-stimulated peak CBV across all time points, including the fluconazole experiments. To further investigate a significant association, a random-effects linear regression model was used to assess each CBV measure versus the paired average 12- and 15-HETE concentration. A significant association was noted that suggests that a doubling of the average 12- and 15-HETE concentration is associated with a 13% increase in the glucose-stimulated peak CBV ($P < 0.05$).

DISCUSSION

Insulin-mediated changes in skeletal muscle blood flow and functional CBV are important in facilitating skeletal muscle glucose uptake and are known to be impaired in IR states (4,5,8–10). In this study, we have temporally correlated skeletal muscle perfusion, endothelial-derived vasodilator pathways, and IR in nonhuman primates in order to characterize the microvascular response during the development of diet-induced obesity. Our correlative data suggest that the skeletal muscle CBV response to diet-induced obesity is complex and involves a dissociation between NO and eicosanoid endothelial-derived vasoregulatory pathways. Early in the development of obesity and IR, an increase occurs in basal and glucose-stimulated CBV that suggests a compensatory response of the vasculature to stabilize the degree of IR. Although correlative, our data suggest that the mediators of this compensatory response are predominantly the lipoxygenase-derived eicosanoid vasodilators and the cytochrome P450 eicosanoids because these compounds progressively increase for 18 months while NO bioavailability progressively declines. After 2 years of an HFD, the abrupt loss of the compensatory increase in the lipoxygenase-derived eicosanoid vasodilators coincided with a drop in skeletal muscle

Table 3—Metabolic profile of rhesus macaques on HFD for >2 years before fluconazole test

Weight, kg	12.8 ± 1.0
Truncal fat, %	37.8 ± 2.8
Basal insulin, μIU/mL	37 ± 10
HOMA-IR	6.5 ± 2.1
Basal glucose, mg/dL	67 ± 4
HbA_{1c}, % (mmol/mol)	6.2 ± 0.2 (44 ± 2)
Insulin AUC, μIU/mL × min	5,373 ± 728
AIR, μIU/mL	130 ± 17
K_G, %/min	2.55 ± 0.3
DI, μIU/mL × %/min	337 ± 63

A separate cohort (N = 5) underwent an additional 2-day study protocol after 33 ± 8 months on the HFD. Data are mean ± SEM.

microvascular blood flow and peak CBV along with progressive worsening of IR.

This study is the first to have characterized the temporal changes in the endothelial-derived eicosanoid vasodilators (EETs, DHETs, and 12- and 15-HETE) in relation to skeletal muscle CBV responses in obesity-related IR. It should be noted that the vasoregulatory pathways of NO, cytochrome P450 eicosanoids, and the lipoxygenase-derived 12- and 15-HETE were selected based on preclinical studies suggesting a link between these endothelial-derived metabolites, microvascular function, and cardiometabolic disease states (13,15,26–28). NO is known to play a major role in normal insulin-mediated capillary recruitment (4,5). During euglycemic hyperinsulinemia, EETs act independently or indirectly through eNOS to produce skeletal muscle capillary recruitment (12). We have additionally demonstrated that abnormalities in both NO and eicosanoid compounds are associated with IR and impaired CBV responses to glucose in a nonobese and weight-matched primate model of inactivity (8).

In this current study, the HFD resulted in obesity and an unexpected paradoxical increase in both the basal and glucose-stimulated skeletal muscle blood flow and CBV. On the basis of the concept that an increase in CBV augments the capillary surface area for insulin and glucose transport, one would have predicted an improvement in glucose homeostasis (an elevated K_G) with these CBV changes. Instead, there was a progression of IR at 4 months, indicated by an increase in the insulin AUC concentration and a simultaneous fall in K_G suggesting a further impairment in glucose homeostasis. These findings suggest that

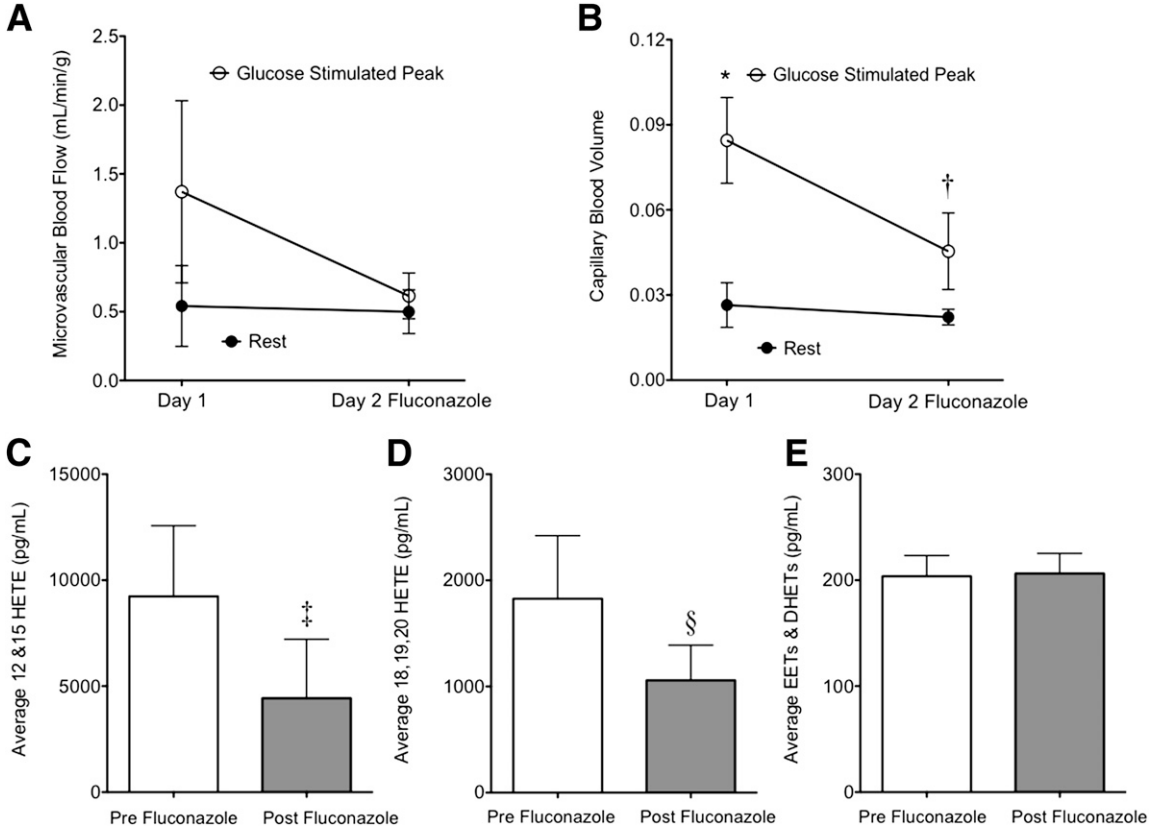

Figure 3—Skeletal muscle microvascular perfusion and eicosanoids in rhesus macaques in response to fluconazole. Microvascular blood flow (*A*) and CBV (*B*). *P < 0.01 vs. rest CBV; †P = 0.03 vs. day 1 peak CBV. *C*: Average 12- and 15-HETE eicosanoid vasodilators. ‡P < 0.05 for pre- vs. postfluconazole values on day 2. *D*: Average 18-, 19-, and 20-HETE eicosanoid vasoconstrictors. §P < 0.01 for pre- vs. postfluconazole values on day 2. *E*: Average eicosanoid vasodilators (8,9-, 11,12-, and 14,15-EETs and corresponding DHETs).

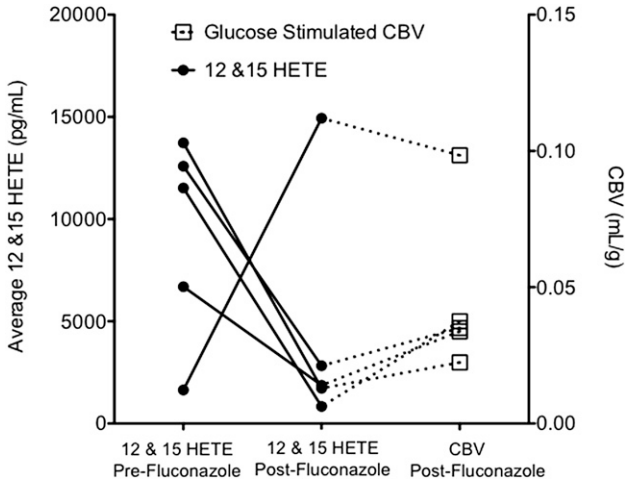

Figure 4—The effect of fluconazole on 12- and 15-HETE concentrations and the relationship to glucose-stimulated CBV.

early in the development of obesity-related IR, eicosanoid-derived vasodilators act as a compensatory mediator to promote expansion of CBV and maintain functional capillary recruitment.

Between 4 and 18 months, the degree of IR stabilized (defined by the plateau phase of insulin secretion and K_G), and skeletal muscle blood flow and CBV at rest and after the glucose challenge remained elevated. During this plateau phase of IR and CBV stability, a further increase occurred in eicosanoid-derived vasodilators (both the cytochrome P450– and lipoxygenase-derived metabolites), but there was a simultaneous decrease in FMD, a measure of NO bioavailability. The shifting pattern of vasodilatory mechanisms suggests that a progressive upregulation of eicosanoid vasodilators may be necessary to maintain the compensatory vascular response to the loss of NO, as previously suggested (26). We did not test whether inhibitors of eicosanoid production reversed the augmentation in functional CBV during the plateau phase because these findings were not anticipated a priori.

At 24 months, there was a simultaneous fall in the resting and glucose-stimulated peak CBV and in the lipoxygenase-derived eicosanoid vasodilators that occurred when IR abruptly worsened. Although the resting and glucose-stimulated peak CBV were not markedly different from baseline values at 24 months, the fall between 18 and 24 months indicates the loss of the preceding compensatory vascular response. This fall in the CBV and the eicosanoid vasodilatory response from the previously compensated state coincided with worsening microvascular IR (reduced glucose-stimulated peak CBV) and appears to contribute to the progression of impaired glucose homeostasis (reduced K_G and DI) in concert with early pancreatic insufficiency (reduced AIR). Furthermore, inhibition of the lipoxygenase-derived 12- and 15-HETE vasodilators in our age-matched, obese primates after 33 months of the HFD clearly demonstrated the relationship between these vasodilators and the ability to augment the skeletal muscle CBV in response to a glucose bolus. In total, these findings lend further support for the protective effect of eicosanoid vasodilators in preserving muscle glucose handling.

The notion that a deficiency in NO can lead to compensatory changes in EDHFs has been suggested in other models of vascular disease (26,29,30). Cytochrome P450–derived EETs and lipoxygenase-derived 12- and 15-HETE vasodilators are upregulated at a time when there is reduced NO availability in hypertension and hypercholesterolemia (31–34). An HFD, hyperglycemia, and elevations of obesity-related cytokines have also been shown to increase 12- and 15-HETE (35–37). That NO is a negative regulator of the production of EDHFs has also been shown (38). Taken together, our data and these previously published data strongly support that a feedback process allows a shift between NO and EDHFs as mediators of vascular tone.

This study has several limitations. Because we are providing temporal correlations of IR, CBV, and eicosanoid-derived vasodilatory pathways, we cannot state with certainty that the increase in CBV during the plateau phase was entirely responsible for stabilization of IR or that the fall in CBV at 2 years was the primary reason for worsening of IR. Our conclusions are instead based on the preponderance of data over the past 15 years indicating that CBV is an important determinant of glucose uptake. Although we believe that the changes in skeletal muscle perfusion and CBV are functional in nature, we have not excluded morphologic changes in capillary density. However, previous studies in rat models of obesity and IR have indicated that reductions in capillary density are very small compared with the reduction in functional CBV (9).

A second limitation is that inhibition of vasodilator EETs and HETEs during the 4- to 18-month plateau phase of IR was not performed to test whether the compensatory responses in CBV were due to these eicosanoid-derived vasodilator compounds and whether they were requisite for stabilizing IR. Our a priori hypothesis was that NO and eicosanoid-vasodilators would both be impaired as obesity and IR develop; thus, the rapid increase in the eicosanoid vasodilator pathways and CBV was unexpected. Furthermore, because the purpose of this study was to temporally characterize endothelial-derived vasodilator pathways and the microvascular response to diet-induced obesity, we did not perform mechanistic studies during the plateau phase because we wanted to understand the natural history of this complex disease process. Alternatively, a mechanistic intervention on age-matched primates with a metabolic and vascular profile similar to obese primates near the end of the plateau phase of IR was performed to demonstrate the effect of eicosanoid-derived vasodilators on functional CBV recruitment.

Additional limitations in the study include the inability to test for endothelin-1, a known potent vasoconstrictor that is upregulated in IR states due to the shift of insulin receptor signaling toward the mitogen-activated protein

kinase pathway and away from the PI3/Akt pathway that promotes NO signaling (39), due to antigen noncross reactivity. For our primary measure of insulin sensitivity, we used the K_G during an IVGTT. Although the hyperinsulinemic-euglycemic clamp can be considered the gold standard to define insulin sensitivity (39–41), the hyperinsulinemic clamp method measures insulin sensitivity at a fixed dose of insulin and does not recapitulate the physiologic surge of insulin in response to an intravenous glucose bolus. Furthermore, the hyperinsulinemic clamp is limited in its capacity to extract data regarding the β-cell function of the pancreas. With the simpler IVGTT, we derived measures of insulin sensitivity (21) as well as the first-phase AIR to assess β-cell function of the pancreas.

Finally, this study lacks a dedicated age, weight, and activity-restricted matched control group on a chow diet to assess the metabolic and skeletal muscle blood flow alterations that may develop over 2 years. Unfortunately, only four animals were preselected as controls in this shared nonhuman primate resource and they were not well matched for age, weight, abdominal adiposity, or time in activity-limited single-cage housing to the animals we monitored. Previous researchers, however, have defined the metabolic characteristics of "successful" and "nonsuccessful" aging in single-caged housed nonhuman primates fed a chow diet (21). Primates that age "successfully" do not go on to develop age-related type 2 diabetes and have no significant changes in insulin sensitivity, AIR, K_G, basal or oral glucose-stimulated plasma insulin and glucose levels, or HbA_{1c} percentage from 10–12 years of age, despite a slight increase in weight and body fat percentage (21). The prespecified "control" group in our shared resource of primates already demonstrated features of "nonsuccessful aging," with multiple features of IR that included elevated truncal fat percentage, increased insulin AUC, and elevated HOMA-IR values. As such, these primates were not serially monitored as a comparative normal and healthy primate cohort.

Conclusions

In this study, we have defined skeletal muscle microvascular responses during the development and progression of IR in diet-induced obesity and have also described the patterns of endothelial-derived vasodilators associated with these changes. The clinical implications of our findings are related to the possibility of developing new vascular-targeted approaches to treating IR because our data suggest that a vascular response can compensate for other mechanisms of abnormal glycemic control for a period of time. There are no currently available therapies focused entirely on maintaining or supporting vascular endothelial function, skeletal muscle blood flow, and CBV responses. The ability to modulate the balance of eicosanoid vasodilators and vasoconstrictors may be valuable for early treatment of IR, a notion that is supported by improved insulin sensitivity found in animal models of metabolic disease (12,42). Future studies using CEU or similar techniques will be needed to better understand the contribution of muscle CBV in clinical trials with these types of agents.

Acknowledgments. The authors thank all of the animal care staff at the Oregon National Primate Research Center and the support staff of the Obese Nonhuman Primate Resource for their excellent animal care and support throughout the study.

Funding. This research was partly supported by a materials grant from Lantheus Medical Imaging. S.M.C. was funded by the American Heart Association Fellow-to-Faculty Award (0875005N) and National Institutes of Health (NIH) grant 5KL2-TR-000152. J.T.B. and P.K. were funded by NIH grant PO1-HD-034430. K.L.G. is supported by NIH grant R01-DK-79194. J.R.L. is supported by NIH grants R01-HL-078610 and R01-HL-111969. The Oregon National Primate Research Center is supported by a National Center for Research Resources grant (S10-RR-024585) and a Research Program Projects and Centers grant (P51-DK-011092) from the NIH. This publication was made possible with support from the Oregon Clinical and Translational Research Institute (OCTRI), grant UL1-RR-024140 from the National Center for Advancing Translational Sciences, a component of the NIH, and NIH Roadmap for Medical Research.

Duality of Interest. No potential conflicts of interest relevant to this article were reported.

Author Contributions. S.M.C. performed data acquisition and data analysis, and wrote, reviewed, and edited the manuscript. S.M.C., K.L.G., and J.R.L. developed the study design. S.M.C. and J.T.B. performed the ultrasound imaging studies. L.B. performed the IVGTTs and DEXA scans. J.T.B., L.B., and P.K. contributed to the data analysis. D.M.P. provided statistical analysis. S.M.C., N.J.A., S.K., K.L.G., and J.R.L. contributed to the discussion and reviewed and edited the manuscript. S.M.C. is the guarantor of this work and, as such, had full access to all the data in the study and takes responsibility for the integrity of the data and the accuracy of the data analysis.

Prior Presentation. Parts of this study were presented in abstract form at the American College of Cardiology 2013 Scientific Sessions, San Francisco, CA, 9–11 March 2013.

References

1. Laakso M, Edelman SV, Brechtel G, Baron AD. Decreased effect of insulin to stimulate skeletal muscle blood flow in obese man. A novel mechanism for insulin resistance. J Clin Invest 1990;85:1844–1852

2. Coggins M, Lindner J, Rattigan S, et al. Physiologic hyperinsulinemia enhances human skeletal muscle perfusion by capillary recruitment. Diabetes 2001;50:2682–2690

3. Dawson D, Vincent MA, Barrett EJ, et al. Vascular recruitment in skeletal muscle during exercise and hyperinsulinemia assessed by contrast ultrasound. Am J Physiol Endocrinol Metab 2002;282:E714–E720

4. Vincent MA, Barrett EJ, Lindner JR, Clark MG, Rattigan S. Inhibiting NOS blocks microvascular recruitment and blunts muscle glucose uptake in response to insulin. Am J Physiol Endocrinol Metab 2003;285:E123–E129

5. Vincent MA, Clerk LH, Lindner JR, et al. Microvascular recruitment is an early insulin effect that regulates skeletal muscle glucose uptake in vivo. Diabetes 2004;53:1418–1423

6. Vincent MA, Clerk LH, Lindner JR, et al. Mixed meal and light exercise each recruit muscle capillaries in healthy humans. Am J Physiol Endocrinol Metab 2006;290:E1191–E1197

7. Vollus GC, Bradley EA, Roberts MK, et al. Graded occlusion of perfused rat muscle vasculature decreases insulin action. Clin Sci (Lond) 2007;112:457–466

8. Chadderdon SM, Belcik JT, Smith E, et al. Activity restriction, impaired capillary function, and the development of insulin resistance in lean primates. Am J Physiol Endocrinol Metab 2012;303:E607–E613

9. Clerk LH, Vincent MA, Barrett EJ, Lankford MF, Lindner JR. Skeletal muscle capillary responses to insulin are abnormal in late-stage diabetes and are

restored by angiotensin-converting enzyme inhibition. Am J Physiol Endocrinol Metab 2007;293:E1804–E1809
10. Clerk LH, Vincent MA, Jahn LA, Liu Z, Lindner JR, Barrett EJ. Obesity blunts insulin-mediated microvascular recruitment in human forearm muscle. Diabetes 2006;55:1436–1442
11. Kim F, Pham M, Maloney E, et al. Vascular inflammation, insulin resistance, and reduced nitric oxide production precede the onset of peripheral insulin resistance. Arterioscler Thromb Vasc Biol 2008;28:1982–1988
12. Shim CY, Kim S, Chadderdon S, et al. Epoxyeicosatrienoic acids mediate insulin-mediated augmentation in skeletal muscle perfusion and blood volume. Am J Physiol Endocrinol Metab 2014;307:E1097–E1104
13. Chawengsub Y, Gauthier KM, Campbell WB. Role of arachidonic acid lipoxygenase metabolites in the regulation of vascular tone. Am J Physiol Heart Circ Physiol 2009;297:H495–H507
14. Larsen BT, Miura H, Hatoum OA, et al. Epoxyeicosatrienoic and dihydroxyeicosatrienoic acids dilate human coronary arterioles via BK(Ca) channels: implications for soluble epoxide hydrolase inhibition. Am J Physiol Heart Circ Physiol 2006;290:H491–H499
15. Mustafa S, Sharma V, McNeill JH. Insulin resistance and endothelial dysfunction: are epoxyeicosatrienoic acids the link? Exp Clin Cardiol 2009;14:e41–e50
16. Ozkor MA, Quyyumi AA. Endothelium-derived hyperpolarizing factor and vascular function. Cardiol Res Pract 2011;2011:156146
17. Bellien J, Iacob M, Gutierrez L, et al. Crucial role of NO and endothelium-derived hyperpolarizing factor in human sustained conduit artery flow-mediated dilatation. Hypertension 2006;48:1088–1094
18. Knights KM, Rowland A, Miners JO. Renal drug metabolism in humans: the potential for drug-endobiotic interactions involving cytochrome P450 (CYP) and UDP-glucuronosyltransferase (UGT). Br J Clin Pharmacol 2013;76:587–602
19. Bremer AA, Stanhope KL, Graham JL, et al. Fructose-fed rhesus monkeys: a nonhuman primate model of insulin resistance, metabolic syndrome, and type 2 diabetes. Clin Transl Sci 2011;4:243–252
20. Chadderdon SM, Belcik JT, Bader L, et al. Proinflammatory endothelial activation detected by molecular imaging in obese nonhuman primates coincides with onset of insulin resistance and progressively increases with duration of insulin resistance. Circulation 2014;129:471–478
21. Tigno XT, Gerzanich G, Hansen BC. Age-related changes in metabolic parameters of nonhuman primates. J Gerontol A Biol Sci Med Sci 2004;59:1081–1088
22. Hansen BC, Bodkin NL. Heterogeneity of insulin responses: phases leading to type 2 (non-insulin-dependent) diabetes mellitus in the rhesus monkey. Diabetologia 1986;29:713–719
23. Kahn SE. Clinical review 135: The importance of beta-cell failure in the development and progression of type 2 diabetes. J Clin Endocrinol Metab 2001; 86:4047–4058
24. Bellien J, Remy-Jouet I, Iacob M, et al. Impaired role of epoxyeicosatrienoic acids in the regulation of basal conduit artery diameter during essential hypertension. Hypertension 2012;60:1415–1421
25. RxList. Fluconazole drug information. Available from http://www.rxlist.com/diflucan-drug/clinical-pharmacology.htm. Accessed 13 November 2015
26. Fleming I. Cytochrome p450 and vascular homeostasis. Circ Res 2001;89: 753–762
27. Natarajan R, Nadler JL. Lipid inflammatory mediators in diabetic vascular disease. Arterioscler Thromb Vasc Biol 2004;24:1542–1548
28. Spector AA, Norris AW. Action of epoxyeicosatrienoic acids on cellular function. Am J Physiol Cell Physiol 2007;292:C996–C1012
29. Clark SG, Fuchs LC. BK(Ca) channels compensate for loss of NOS-dependent coronary artery relaxation in cardiomyopathy. Am J Physiol Heart Circ Physiol 2000;279:H2598–H2603
30. Miura H, Wachtel RE, Liu Y, et al. Flow-induced dilation of human coronary arterioles: important role of Ca(2+)-activated K(+) channels. Circulation 2001; 103:1992–1998
31. Pfister SL, Falck JR, Campbell WB. Enhanced synthesis of epoxyeicosatrienoic acids by cholesterol-fed rabbit aorta. Am J Physiol 1991;261:H843–H852
32. Pritchard KA Jr, Wong PY, Stemerman MB. Atherogenic concentrations of low-density lipoprotein enhance endothelial cell generation of epoxyeicosatrienoic acid products. Am J Pathol 1990;136:1383–1391
33. Stapleton PA, Goodwill AG, James ME, Frisbee JC. Altered mechanisms of endothelium-dependent dilation in skeletal muscle arterioles with genetic hypercholesterolemia. Am J Physiol Regul Integr Comp Physiol 2007;293:R1110–R1119
34. Yu Z, Huse LM, Adler P, et al. Increased CYP2J expression and epoxyeicosatrienoic acid formation in spontaneously hypertensive rat kidney. Mol Pharmacol 2000;57:1011–1020
35. Chen M, Yang ZD, Smith KM, Carter JD, Nadler JL. Activation of 12-lipoxygenase in proinflammatory cytokine-mediated beta cell toxicity. Diabetologia 2005;48:486–495
36. Natarajan R, Gu JL, Rossi J, et al. Elevated glucose and angiotensin II increase 12-lipoxygenase activity and expression in porcine aortic smooth muscle cells. Proc Natl Acad Sci U S A 1993;90:4947–4951
37. Nunemaker CS, Chen M, Pei H, et al. 12-Lipoxygenase-knockout mice are resistant to inflammatory effects of obesity induced by Western diet. Am J Physiol Endocrinol Metab 2008;295:E1065–E1075
38. Bauersachs J, Popp R, Hecker M, Sauer E, Fleming I, Busse R. Nitric oxide attenuates the release of endothelium-derived hyperpolarizing factor. Circulation 1996;94:3341–3347
39. Kim JA, Montagnani M, Koh KK, Quon MJ. Reciprocal relationships between insulin resistance and endothelial dysfunction: molecular and pathophysiological mechanisms. Circulation 2006;113:1888–1904
40. Amati F, Dubé JJ, Coen PM, Stefanovic-Racic M, Toledo FG, Goodpaster BH. Physical inactivity and obesity underlie the insulin resistance of aging. Diabetes Care 2009;32:1547–1549
41. Shen SW, Reaven GM, Farquhar JW. Comparison of impedance to insulin-mediated glucose uptake in normal subjects and in subjects with latent diabetes. J Clin Invest 1970;49:2151–2160
42. Iyer A, Kauter K, Alam MA, et al. Pharmacological inhibition of soluble epoxide hydrolase ameliorates diet-induced metabolic syndrome in rats. Exp Diabetes Res 2012;2012:758614